Journal of Zhejiang University-SCIENCE A (Applied Physics & Engineering)
ISSN 1673-565X (Print); ISSN 1862-1775 (Online)
www.zju.edu.cn/jzus; www.springerlink.com
E-mail: jzus@zju.edu.cn

Nonlinear dynamic analysis of a rotor/bearing/seal system*

Wei LI†, Yi YANG, De-ren SHENG, Jian-hong CHEN, Yong-qiang CHE

(*Department of Energy Engineering, Zhejiang University, Hangzhou 310027, China*)

†E-mail: Energy@zju.edu.cn

Received Mar. 31, 2010; Revision accepted Sept. 29, 2010; Crosschecked Dec. 10, 2010

Abstract: In this study a new dynamic model of a rotor system is established based on the Hamilton principle and the finite element method (FEM). We analyze the dynamic behavior of the rotor system with the coupled effects of the nonlinear oil film force, the nonlinear seal force, and the mass eccentricity of the disk. The equations of the motion are solved effectively using the fourth order Runge-Kutta method in MATLAB. The dynamic behavior of the system is illustrated by bifurcation diagrams, largest Lyapunov exponents, phase trajectory diagrams, and Poincaré maps. The numerical results show that the rotational speed of the rotor, the pressure drop in the seal, the seal length, the seal clearance, and the mass eccentricity of the disk are the key parameters that significantly affect the dynamic characteristics of the rotor system. The motion of the rotor system exhibits complex types of periodic, quasi-periodic, double-periodic, multi-periodic, and chaotic vibrations. This analysis can be used to guide the design of seal parameters and to diagnose the vibration of rotor/bearing/seal systems.

Key words: Nonlinear, Rotor system, Hamilton principle, Dynamic, Finite element method (FEM)
doi:10.1631/jzus.A1000130 **Document code:** A **CLC number:** TH117.2

1 Introduction

Nonlinear systems such as the rotor system have recently been the subject of considerable scientific and engineering study. The rotor system is a nonlinear system and should be analyzed using a nonlinear method. The rotor/bearing/seal system, which is subject to a strong aerodynamic force induced by the leakage flow through the seals, may exhibit nonlinear behavior in its orbital motion (Wang *et al.*, 2009). Thus, research on the influence of the nonlinear seal force on the dynamic characteristics of the rotor system is of great importance.

Many studies have focused on the analysis of rotor system dynamics or related research. Wang *et al.* (1999) constructed a nonlinear dynamic model of a continuous rotor system under the action of a bearing oil film force based on the Hamilton principle. Al-Nahwi *et al.* (2003) investigated the principle and interaction of steam excitation on the Jeffcott rotor system using a combined Moore-Greitzer flow field model. Shen (2007) developed software which can analyze the dynamics and stability of a rotor system of large scale turbines, based on the finite element method (FEM). Huang *et al.* (2007) considered the combined effect of steam excited force in the blade tip and bearing oil film force, and analyzed the system response by solving the dimensionless dynamic equations. Luo *et al.* (2007) built a periodical time-variable high-dimensional dynamic rotor system based on the FEM and used the shooting method to analyze the rotor stability. Li (2007) established a nonlinear dynamic model of an unbalanced rotor system, and applied the shooting method and Floquet theory to study the dynamic behavior of the periodic solutions. Cheng *et al.* (2007a; 2008) set up a dynamic model of the nonlinear rotor system combining the nonlinear bearing force and seal force models. The nonlinear dynamic behavior of the coupled system was studied using the numerical value integral method (Cheng *et al.*, 2007b; 2008). Wang *et al.* (2009) established a nonlinear mathematical model

* Project (No. Y107356) supported by the Zhejiang Provincial Natural Science Foundation of China

for orbital motion of the rotor system under the influence of leakage flow through an interlocking seal. Particular attention was placed on the serpentine flow path by spatially separating the aerodynamic force on the rotor surface into the seal clearance and the cavity volume. Chang-Jian and Chen (2006a; 2006b; 2007a; 2007b) and Chang-Jian (2010a; 2010b) presented a series of papers about a rotor supported by journal bearings under nonlinear suspension or combined with a rub-impact effect, a turbulent effect and a micropolar lubricant. Wang and Wang (2010) analyzed the nonlinear coupling vibration and bifurcation of a high-speed centrifugal compressor with a labyrinth seal and two air film journal bearings. They presented bifurcation diagrams for transverse motion of the rotor with the parameters of rotation speed and the pressure drop of the seal.

Though the previous studies emphasized the dynamic behavior of the rotor system, no nonlinear model of the rotor/bearing/seal system with the coupled effects of the nonlinear oil film force and the seal force based on the Hamilton principle was developed. In this paper, a new dynamic model of the rotor/bearing/seal system is established based on the Hamilton principle and FEM, considering the coupled effects of the nonlinear oil film force, the nonlinear seal force, and the mass eccentricity of the disk. The equations of motion are solved using the fourth order Runge-Kutta method. The dynamic behaviors of this rotor system are illustrated by bifurcation diagrams, Lyapunov exponents, phase trajectory diagrams, and Poincaré maps. In addition, this study focuses specifically on the effect of the rotational speed of the rotor, the pressure drop in the seal, the seal length and clearance, and the mass eccentricity of the disk.

2 Mathematical model of the rotor/bearing/seal system

In this section, a new nonlinear model of a rotor/bearing/seal system is established based on the Hamilton principle and FEM. Fig. 1 is a schematic of a simplified geometric model for a rotor/bearing/seal system, which is modeled as a rigid Jeffcott rotor system. The seal force acts on the disk, and two oil film forces act on each end of the rotor.

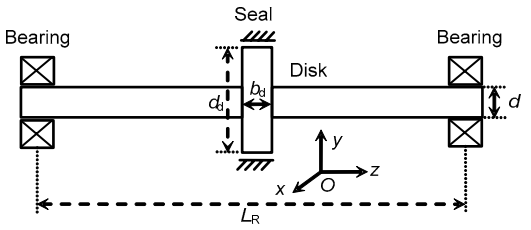

Fig. 1 Sketch map of a rotor/bearing/seal system
L_R is the length of rotor, d_d is the diameter of the disk, d is the diameter of the shaft, and b_d is the width of the disk

Firstly, based on the Timoshenko theory (Zeng, 2004), the finite element model of the rotor/bearing/seal system can be established as shown in Fig. 2. There are a total of four shaft units and five nodes. Each node has four degrees of freedom including two rotational displacements and two translational displacements. The disk mass acts at node 3 as a concentrated mass, nodes 1 and 5 are journal bearings, and nodes 2 and 4 are at points at one quarter and three quarters, respectively, of the length of the rotor.

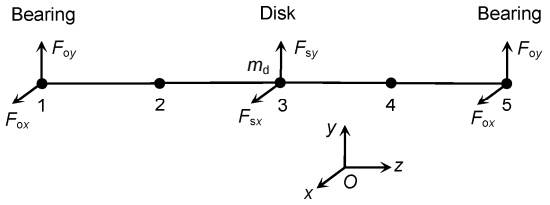

Fig. 2 Finite element model of a rotor system
m_d is the disk mass; F_{ox} and F_{oy} are the oil film forces in the x and y directions, respectively; F_{sx} and F_{sy} are the seal film forces in the x and y directions, respectively

Then the kinetic and potential energy equations of the shaft units and the disk will be derived using the projected angle method. The fixed coordinate system O-xyz can be established with the disk center O as the origin. When there is no disk deformation caused by the disturbance, the center axis of the disk is along the z axis. When the barycenter of the disk deviates from the origin point O, a rotary coordinate system O-$\xi\eta\zeta$ can be established, with ζ axis as the center axis of the disk, and an angle θ with the positive z axis (Fig. 3). The angular displacements θ_x and θ_y are defined as the angles between the z axis and the projection of the ζ axis onto the xz and yz planes, respectively. Let line OP be perpendicular to the $z\zeta$ plane from point O. The coordinate system O-$\xi\eta\zeta$ can be obtained by first rotating around OP by angle θ from the O-xyz system,

and then rotating around ζ axis by angle ϕ, where ϕ is the disk rotation angle.

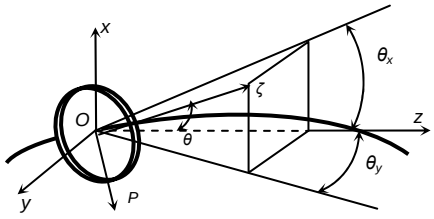

Fig. 3 Sketch map of the rotary coordinate

The kinetic energy T_s and the strain energy U_s of the shaft units can be expressed as follows (Zhang, 1990):

$$T_s = \int_0^l \frac{1}{2}\rho\left\{A(\dot{x}^2+\dot{y}^2)+I_{\mathrm{d}}(\dot{\theta}_x^2+\dot{\theta}_y^2) +I_{\mathrm{p}}\left[\Omega^2+\Omega(\dot{\theta}_x\theta_y-\dot{\theta}_y\theta_x)\right]\right\}\mathrm{d}s, \tag{1}$$

$$U_s = \int_0^l \frac{1}{2}\left\{EI\left[(\theta_x')^2+(\theta_y')^2\right] + kGA\left[(\theta_y-x')^2+(\theta_x+y')^2\right]\right\}\mathrm{d}s, \tag{2}$$

where $x'=\dfrac{\partial x}{\partial s}$, $y'=\dfrac{\partial y}{\partial s}$, $\theta_x'=\dfrac{\partial \theta_x}{\partial s}$, $\theta_y'=\dfrac{\partial \theta_y}{\partial s}$, ρ is the material density, l is the length of the shaft unit, x and y are the translational displacements in the x and y directions, respectively, θ_x and θ_y are the rotational displacements in the x and y directions, respectively, Ω is the rotational speed, A is the sectional area of the shaft unit, E is Young's modulus of elasticity, I_{d} is the diametric inertia moment of the shaft unit, I_{p} is the polar inertia moment of the shaft unit, k is the shape factor, and G is the shear modulus.

The kinetic energy of the disk can be written as

$$T_{\mathrm{d}} = \frac{1}{2}m_{\mathrm{d}}(\dot{x}^2+\dot{y}^2)+\frac{1}{2}J_{\mathrm{d}}(\dot{\theta}_x^2+\dot{\theta}_y^2) +\frac{1}{2}J_{\mathrm{p}}\left[\Omega^2+\Omega(\dot{\theta}_x\theta_y-\dot{\theta}_y\theta_x)\right], \tag{3}$$

where m_{d} is the disk mass, J_{d} is the diametric rotary inertia of the disk, and J_{p} is the polar rotary inertia of the disk.

The work caused by the nonconservative forces is expressed as follows:

$$W = \sum_{i=1}^{n} F_i q_i, \tag{4}$$

where F_i is the nonconservative force, such as the seal force, the oil-film force, and the mass eccentricity force, and q_i is the displacement under the force F_i.

The Hamilton principle states that, during the true evolution of a conservative holonomic system, the variation of the Hamilton action equals 0 (Mei and Liu, 1987). This can be written as

$$\delta S = \delta\int_{t_0}^{t_1} L\mathrm{d}t = \delta\int_{t_0}^{t_1}(T-U)\mathrm{d}t = 0, \tag{5}$$

where t_0 and t_1 are the times at the beginning and the end, respectively, of a time step, L is the Lagrangian function, T is the kinetic energy of the system, and U is the potential energy of the rotor system.

For a general holonomic system, the extended Hamilton principle can be expressed as

$$\delta\int_{t_0}^{t_1}(T-U+W)\mathrm{d}t = 0\,. \tag{6}$$

For a rotor/bearing/seal system, which is a holonomic nonconservative system, the motion equation of the shaft units can be obtained based on the extended Hamilton principle by substituting Eqs. (1), (2) and (4) into Eq. (6):

$$\boldsymbol{M}_{\mathrm{e}}\ddot{\boldsymbol{q}}_{\mathrm{e}} + (\Omega\boldsymbol{\Omega}_{\mathrm{e}}+\boldsymbol{C}_{\mathrm{e}})\dot{\boldsymbol{q}}_e + \boldsymbol{K}_{\mathrm{e}}\boldsymbol{q}_{\mathrm{e}} = \boldsymbol{F}_{\mathrm{e}}+\boldsymbol{G}_{\mathrm{e}}, \tag{7}$$

where $\boldsymbol{M}_{\mathrm{e}}$ is the mass matrix, $\boldsymbol{q}_{\mathrm{e}}$ is the nodal displacement vector, $\boldsymbol{\Omega}_{\mathrm{e}}$ is the gyroscope matrix, $\boldsymbol{C}_{\mathrm{e}}$ is the damping matrix, $\boldsymbol{K}_{\mathrm{e}}$ is the stiffness matrix, $\boldsymbol{F}_{\mathrm{e}}$ is the vector of forces acting on the shaft unit, and $\boldsymbol{G}_{\mathrm{e}}$ is the gravitation vector. The subscript 'e' denotes the shaft unit, and 'd' denotes the disk. No subscript denotes the rotor system.

Similarly, the differential equations of motion for the disk can be obtained by substituting Eqs. (3) and (4) into Eq. (6) if the mass eccentricity of the disk is considered.

$$\boldsymbol{M}_{\mathrm{d}}\ddot{\boldsymbol{q}}_{\mathrm{d}} + (\Omega\boldsymbol{\Omega}_{\mathrm{d}}+\boldsymbol{C}_{\mathrm{d}})\dot{\boldsymbol{q}}_{\mathrm{d}} = \boldsymbol{F}_{\mathrm{d}}+\boldsymbol{G}_{\mathrm{d}}, \tag{8}$$

where

$$\boldsymbol{M}_{\mathrm{d}}=\begin{bmatrix} m_{\mathrm{d}} & & & \\ & m_{\mathrm{d}} & & \\ & & J_{\mathrm{d}} & \\ & & & J_{\mathrm{d}} \end{bmatrix},\quad \boldsymbol{\Omega}_{\mathrm{d}}=\begin{bmatrix} 0 & & & \\ & 0 & & \\ & & 0 & J_{\mathrm{p}} \\ & & -J_{\mathrm{p}} & 0 \end{bmatrix}.$$

The equations of motion of the rotor/bearing/seal system can be achieved by assembling all shaft units and the disk as follows:

$$\boldsymbol{M}\ddot{\boldsymbol{q}}+\left(\Omega\boldsymbol{\Omega}+\boldsymbol{C}\right)\dot{\boldsymbol{q}}+\boldsymbol{K}\boldsymbol{q}=\boldsymbol{F}+\boldsymbol{G}, \tag{9}$$

where $\boldsymbol{q}=[x_1, y_1, x_2, y_2, x_3, y_3, x_4, y_4, x_5, y_5]^{\mathrm{T}}$, $\boldsymbol{F}=[F_{ox}, F_{oy}, 0, 0, F_{sx}+F_{dx}, F_{sy}+F_{dy}, 0, 0, F_{ox}, F_{oy}]^{\mathrm{T}}$, $F_{dx}=m_{\mathrm{d}}r_{\mathrm{d}}\Omega^2\cos(\Omega t)$, and $F_{dy}=m_{\mathrm{d}}r_{\mathrm{d}}\Omega^2\sin(\Omega t)$.

Then the equations of motion for the rotor system can be nondimensionalized for easier derivation. We can define the dimensionless displacement $\boldsymbol{Q}$ and dimensionless time τ as

$$\boldsymbol{Q}=\frac{\boldsymbol{q}}{c_{\mathrm{o}}}=[X_1, Y_1, X_2, Y_2, X_3, Y_3, X_4, Y_4, X_5, Y_5]^{\mathrm{T}},$$
$$\tau=\Omega t. \tag{10}$$

Therefore, Eq. (9) can be transformed as

$$\Omega^2 c_{\mathrm{o}}\boldsymbol{M}\ddot{\boldsymbol{Q}}+\Omega c_{\mathrm{o}}(\Omega\boldsymbol{\Omega}+\boldsymbol{C})\dot{\boldsymbol{Q}}+c_{\mathrm{o}}\boldsymbol{K}\boldsymbol{Q}=\boldsymbol{F}+\boldsymbol{G}, \tag{11}$$

where c_{o} is the average clearance of bearing.

For simplicity, the short bearing oil film force model is applied to describe the nonlinear oil film force, and its dimensionless form can be written as

$$\begin{bmatrix} F'_{ox} \\ F'_{oy} \end{bmatrix}=\frac{1}{\sigma}\begin{bmatrix} F_{ox} \\ F_{oy} \end{bmatrix} =\frac{1}{2}\begin{bmatrix} C_2 & -C_3 \\ C_3 & C_2 \end{bmatrix}\begin{bmatrix} X \\ Y \end{bmatrix}-\begin{bmatrix} C_{11} & C_{12} \\ C_{21} & C_{22} \end{bmatrix}\begin{bmatrix} \dot{X} \\ \dot{Y} \end{bmatrix}, \tag{12}$$

where $\sigma=\mu\Omega R_{\mathrm{o}}L_{\mathrm{o}}\left(\frac{R_{\mathrm{o}}}{c_{\mathrm{o}}}\right)^2\left(\frac{L_{\mathrm{o}}}{2R_{\mathrm{o}}}\right)^2$, F_{ox} and F_{oy} are the oil film forces in the x and y directions, respectively. The detailed expressions of C_1, C_2, C_3, C_{11}, C_{12}, C_{21}, and C_{22} can be found in Xu and Zhang (2000).

The Muszynska model is used to describe the nonlinear seal force because it is able to describe well the nonlinear characteristic of seal force (Muszynska and Bently, 1990). Its dimensionless form can be written as

$$\begin{bmatrix} F_{sx} \\ F_{sy} \end{bmatrix}=-c_{\mathrm{o}}\begin{bmatrix} K-m_{\mathrm{f}}\tau_{\mathrm{f}}^2\Omega^2 & \tau_{\mathrm{f}}\Omega D \\ -\tau_{\mathrm{f}}\Omega D & K-m_{\mathrm{f}}\tau_{\mathrm{f}}^2\Omega^2 \end{bmatrix}\begin{bmatrix} X_3 \\ Y_3 \end{bmatrix} -\Omega c_{\mathrm{o}}\begin{bmatrix} D & 2\tau_{\mathrm{f}}\Omega m_{\mathrm{f}} \\ 2\tau_{\mathrm{f}}\Omega m_{\mathrm{f}} & D \end{bmatrix}\begin{bmatrix} \dot{X}_3 \\ \dot{Y}_3 \end{bmatrix} -\Omega^2 c_{\mathrm{o}}\begin{bmatrix} m_{\mathrm{f}} & 0 \\ 0 & m_{\mathrm{f}} \end{bmatrix}\begin{bmatrix} \ddot{X}_3 \\ \ddot{Y}_3 \end{bmatrix}, \tag{13}$$

where τ_{f} is the average circumferential velocity ratio of fluid, and K, D, and m_{f} are the equivalent stiffness, damping, and mass, respectively, of fluid.

If we make $\boldsymbol{M}'=\boldsymbol{M}+\mathrm{diag}\{0, 0, 0, 0, m_{\mathrm{f}}, m_{\mathrm{f}}, 0, 0, 0, 0\}$, the dimensionless equations of motion can be obtained as

$$\ddot{\boldsymbol{Q}}+\frac{\Omega\boldsymbol{\Omega}+\boldsymbol{C}}{\Omega\boldsymbol{M}'}\dot{\boldsymbol{Q}}+\frac{\boldsymbol{K}}{\Omega^2\boldsymbol{M}'}\boldsymbol{Q}=\frac{\boldsymbol{F}'+\boldsymbol{G}}{\Omega^2 c_{\mathrm{o}}\boldsymbol{M}'}, \tag{14}$$

where

$$\boldsymbol{F}'=[\sigma F'_{ox}, \sigma F'_{oy}, 0, 0, F'_{sx}+F_{dx}, F'_{sy}+F_{dy}, 0, 0, \sigma F'_{ox}, \sigma F'_{oy}]^{\mathrm{T}},$$
$$\begin{bmatrix} F'_{sx} \\ F'_{sy} \end{bmatrix}=-c_{\mathrm{o}}\begin{bmatrix} K-m_{\mathrm{f}}\tau_{\mathrm{f}}^2\Omega^2 & \tau_{\mathrm{f}}\Omega D \\ -\tau_{\mathrm{f}}\Omega D & K-m_{\mathrm{f}}\tau_{\mathrm{f}}^2\Omega^2 \end{bmatrix}\begin{bmatrix} X_3 \\ Y_3 \end{bmatrix} -\Omega c_{\mathrm{o}}\begin{bmatrix} D & 2\tau_{\mathrm{f}}\Omega m_{\mathrm{f}} \\ 2\tau_{\mathrm{f}}\Omega m_{\mathrm{f}} & D \end{bmatrix}\begin{bmatrix} \dot{X}_3 \\ \dot{Y}_3 \end{bmatrix}.$$

Eq. (14) describes a nonlinear dynamic model of the rotor/bearing/seal system. The numerical solutions of this nonlinear equation can be obtained using the fourth order Runge-Kutta method.

3 Numerical results and discussion

3.1 Analytical methods

To illustrate the nonlinear dynamics of the rotor system, bifurcation diagrams, largest Lyapunov exponents, phase trajectory diagrams, and Poincaré maps are used. These classical analytical methods will be briefly introduced as follows.

1. Bifurcation diagrams. A bifurcation diagram captures the essential dynamics of a rotor system. It is

a useful tool in that we can understand the system by observing its nonlinear dynamic response. In the present analysis, the bifurcation diagrams are generated using two control parameters, namely the rotational speed Ω, and the dimensionless displacement in the x or y direction, X or Y, respectively. Then the variation of return points in the Poincaré map of dimensionless time can be plotted against the control parameter.

2. Largest Lyapunov exponents. Lyapunov exponents quantify the exponential divergence of the initially close state-space trajectories, and estimate the amount of chaos in a system. The usual test for chaos is by the calculation of the largest Lyapunov exponent. A positive largest Lyapunov exponent indicates chaos. If the largest value is equal to zero, it indicates periodic or quasi-periodic dynamics (Rosenstein *et al.*, 1993). If all Lyapunov exponents are negative, then the stable critical point is an attractor.

3. Phase trajectory diagrams. By numerical integration of the equations of rotor motion, the y coordinate, which denotes the dimensionless speed in the x or y direction, can be plotted against the x coordinate which stands for the dimensionless displacement in the x or y direction as time increases.

4. Poincaré maps. A Poincaré map can be interpreted as a discrete dynamical system with a state space that is one dimension smaller than the original continuous dynamical system. Since it preserves many properties of the periodic and quasi-periodic orbits of the original system, it is often used to investigate periodic or quasi-periodic dynamical systems. A Poincaré section is a stroboscopic picture of the motion in a phase plane, and consists of points time-wise at a constant interval of T ($T=2\pi/\Omega$). A point on a Poincaré section is referred to as a return point. The projection of a Poincaré section on the $X(nT)$-$Y(nT)$ plane is referred to as a Poincaré map of the motion (Cheng *et al.*, 2007b).

3.2 Numerical analysis and results

Because of the strong nonlinearity of the rotor system coupling with the nonlinear oil film force and the nonlinear seal force, the dimensionless equations of motion are difficult to solve using conventional perturbation methods. In this study, the numerical analysis was performed using the fourth order Runge-Kutta method with adaptive step control to reduce the local truncation error of every step. The partial test parameters of the numerical calculation are given in Table 1. In the numerical calculation, the ODE45 solver in MATLAB was employed, which gives the user limited control over the algorithm. The initial displacements and velocities of the disk center and the two bearings were 0.01. The dimensionless time ranged from 0 to 800π, and the time step was 0.01π. Thus, 80001 data points could be obtained. The latter 40001 data points were plotted, while the first 40000 were discarded considering the iteration veracity.

Table 1 Partial test parameters

Structural parameter	Value	Structural parameter	Value
Length of rotor (m)	1.0	Rotor density (kg/m^3)	7810
Length of the shaft unit (m)	0.25	Clearance of the bearing (m)	0.0002
Diameter of the shaft (m)	0.05	Length of the bearing (m)	0.0252
Diameter of the disk (m)	0.5	Radius of the bearing (m)	0.0252
Length of the seal (m)	0.052	Clearance of the seal (m)	0.001
Mass eccentricity of the disk (m)	0.00006		

3.2.1 Impact of the rotational speed

Rotational speed is one of the important parameters that affect the dynamic response of a rotor system. Fig. 4 shows the bifurcation diagrams and Lyapunov exponents of the dimensionless displacement X at the bearings and the disk. The rotational speed is used as the control parameter, and ranges from 80 to 1000 rad/s. The response of the rotor system becomes more complicated with increasing rotational speed. There is only one point in the bifurcation diagram (Figs. 4a and 4b), and the rotor system is in motion of period-one when $\Omega<343$ rad/s. The period-one motion loses its stability and a typical period doubling bifurcation takes place at $\Omega=343$ rad/s, and correspondingly the largest Lyapunov exponents (Figs. 4c and 4d) change their values from negative to zero. The motion of the system then remains double-periodic until the quasi-period bifurcation occurs at $\Omega=458$ rad/s. The motion of the system remains

quasi-periodic in the range [458, 584] rad/s. Fig. 4 shows that the dynamics of the system change and the motion becomes chaotic at Ω=584 rad/s, which is reflected by the largest Lyapunov exponents being positive. The chaotic motion is random and seemingly out of order, and cannot be forecasted for long term. The motions of the bearings and the disk then return to quasi-periodic at Ω=648 rad/s, as shown by the largest Lyapunov exponents. As the rotational speed gradually increases, the motions appear quintuple-periodic in the range [656, 712] rad/s. Finally, the motions shift between quasi-periodic and multi-periodic when $\Omega \geq 712$ rad/s.

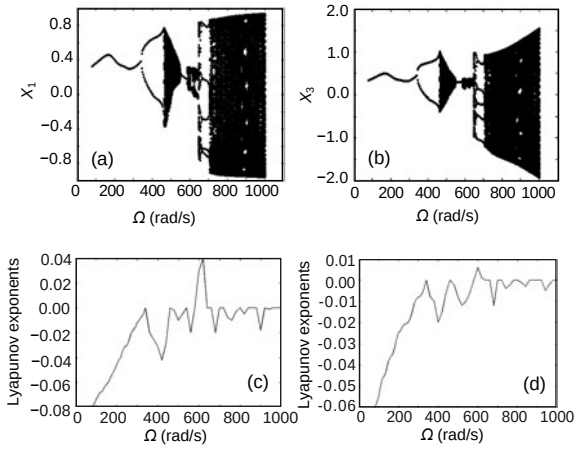

Fig. 4 Bifurcation diagram at the left bearing (a) and at the disk (b), Lyapunov exponents at the left bearing (c) and at the disk (d) of the rotor system

The Poincaré maps and the phase trajectory diagrams of the disk under different rotational speeds are plotted in Figs. 5–10. For convenience, only the data of the dimensionless translation displacement in the x direction were used to generate the diagrams. Fig. 5 presents the dynamic characteristics of the rotor system at Ω=300 rad/s. The disk is synchronous to the period-one motion when the rotation is slow and only one corresponding point is shown in the Poincaré map (Fig. 5a). At Ω=400 rad/s (Fig. 6), there are two isolated points in the Poincaré maps which collectively represent the double-periodic motion. At Ω=500 rad/s (Fig. 7), the figures represent the quasi-periodic motion and the phase trajectory diagram shows irregular motion. There is a closed curve in the Poincaré maps. At Ω=600 rad/s (Fig. 8), the figures represent chaotic motion, not following any discernable regular pattern but varying in an unpredictable way. There are two isolated closed curves in the Poincaré maps and the phase trajectory is irregular. At Ω=700 rad/s (Fig. 9), there are five isolated points in the Poincaré maps and the phase trajectory diagrams show quintuple-periodic motion. At Ω=800 rad/s (Fig. 10), a closed curve in the Poincaré maps and irregular motion in the phase trajectory diagram of the disk demonstrate typical quasi-periodic motion.

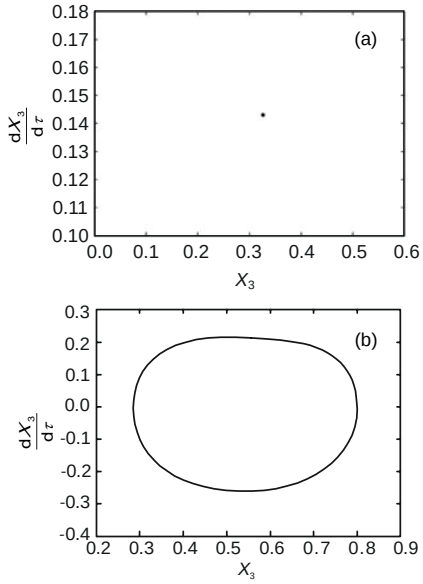

Fig. 5 Responses of the rotor at the disk at Ω=300 rad/s
(a) Poincaré map; (b) Phase trajectory diagram

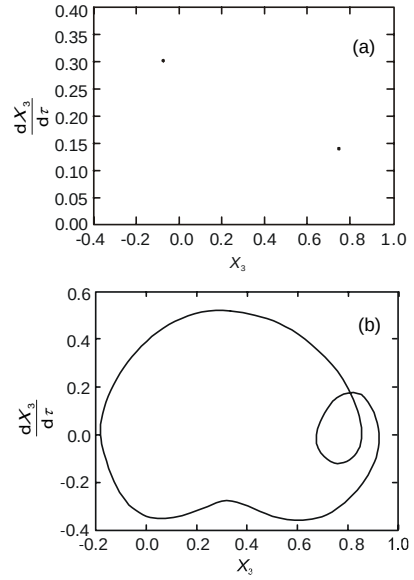

Fig. 6 Responses of the rotor at the disk at Ω=400 rad/s
(a) Poincaré map; (b) Phase trajectory diagram

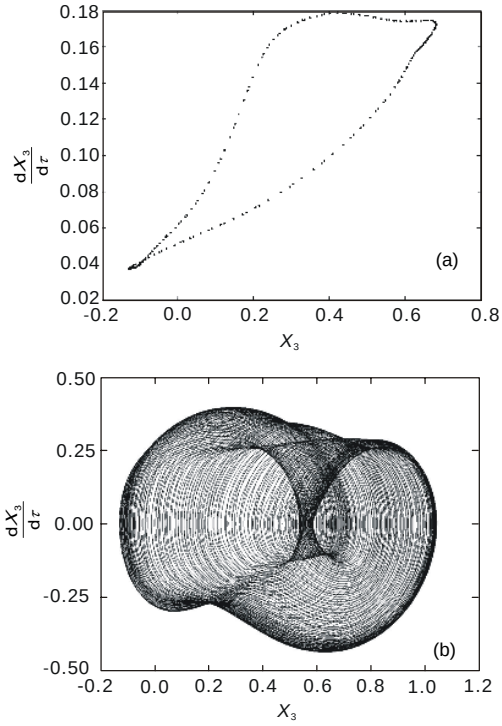

Fig. 7 Responses of the rotor at the disk at Ω=500 rad/s
(a) Poincaré map; (b) Phase trajectory diagram

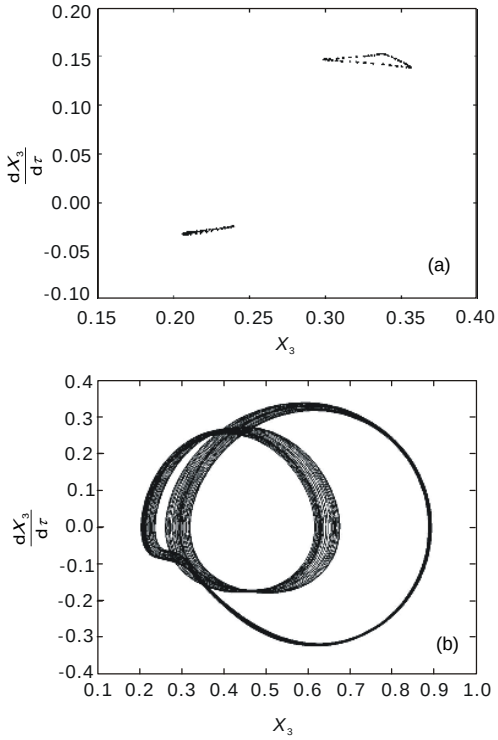

Fig. 8 Responses of the rotor at the disk at Ω=600 rad/s
(a) Poincaré map; (b) Phase trajectory diagram

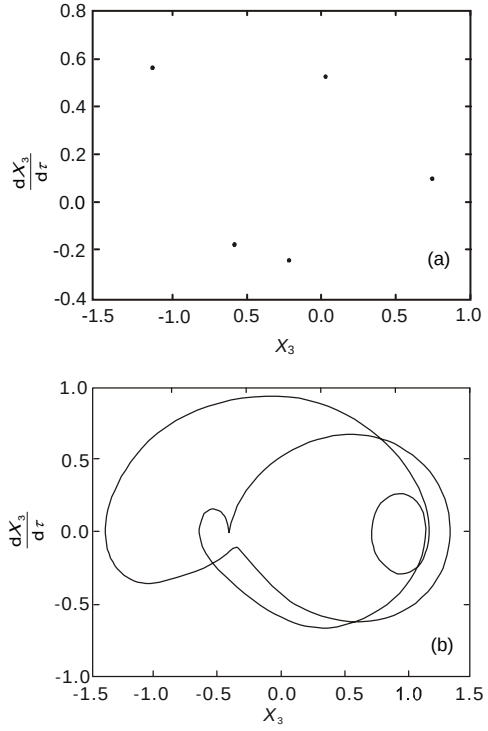

Fig. 9 Responses of the rotor at the disk at Ω=700 rad/s
(a) Poincaré map; (b) Phase trajectory diagram

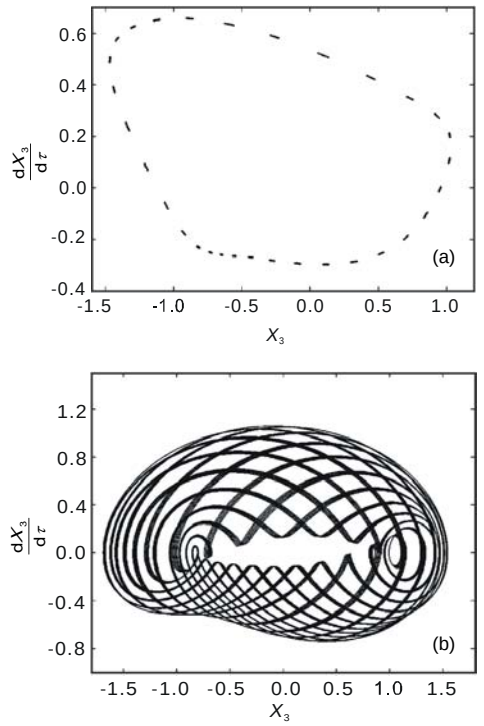

Fig. 10 Responses of the rotor at the disk at Ω=800 rad/s
(a) Poincaré map; (b) Phase trajectory diagram

For the analysis of the specific effects on the rotor dynamic characteristic of the pressure drop in seal (Δp), the seal length (L_s), the seal clearance (c_s), and the mass eccentricity of disk (r_d), different bifurcation diagrams were obtained with different parameters under some rotational speed (i.e., Ω= 480 rad/s).

3.2.2 Impact of the pressure drop Δp

Fig. 11 shows the bifurcation diagrams obtained when the pressure drop in the seal is adopted as the bifurcation parameter and ranges from 0.2 to 1.0 MPa, for r_d=0.06 mm, L_s=52 mm, and c_s=1 mm. The characteristics of the system motion can be generalized as follows: quasi-periodic motion alternating with multi-periodic motion→quasi-periodic motion→periodic motion. The diagrams show that the increase in the pressure drop leads to system instability and the motion state changes frequently when $\Delta p \leq 0.49$ MPa. With increasing Δp (Δp>0.49 MPa), the amplitude of the system decreases and the system returns to periodic motion when the pressure drop is higher than 0.7 MPa.

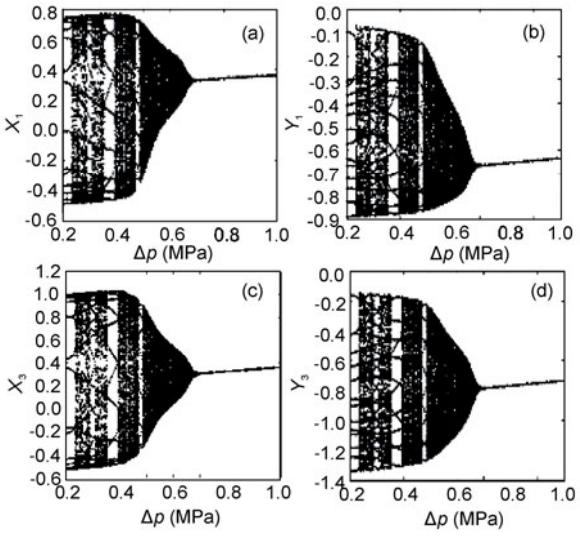

Fig. 11 Bifurcation behavior of the rotor with increasing pressure drop
(a) Bifurcation of *x*-response at the bearing; (b) Bifurcation of *y*-response at the bearing; (c) Bifurcation of *x*-response at the disk; (d) Bifurcation of *y*-response at the disk

3.2.3 Impact of the seal clearance c_s

Fig. 12 shows the bifurcation diagrams obtained when the seal clearance is adopted as the bifurcation parameter and ranges from 0.1 to 2 mm, for r_d=0.06 mm, L_s=52 mm, and Δp=0.5 MPa. With increasing c_s, the motion characteristics can be described as: double-periodic motion→periodic motion →quasi-periodic motion→multi-periodic motion alternating with quasi-periodic motion and chaotic motion. Under these conditions, the double periodic motion is limited when c_s=0.28 mm and the system maintains periodic motion in the range [0.28, 0.42] mm. However, at larger seal clearances (c_s> 0.42 mm), the amplitude of the system increases rapidly, and the system demonstrates more complicated motion.

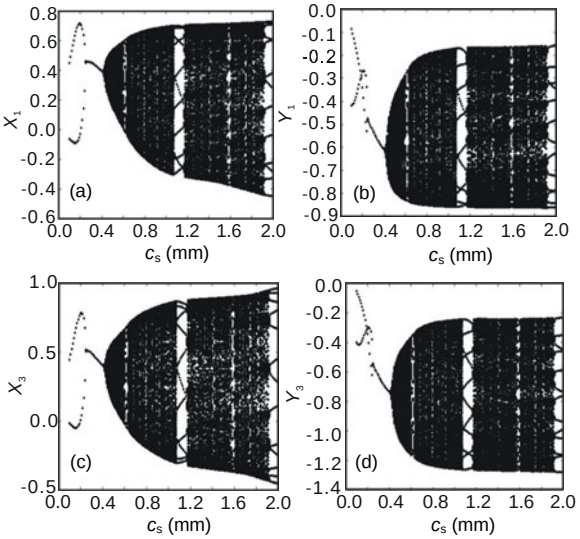

Fig. 12 Bifurcation behavior of the rotor with increasing seal clearance
(a) Bifurcation of *x*-response at the bearing; (b) Bifurcation of *y*-response at the bearing; (c) Bifurcation of *x*-response at the disk; (d) Bifurcation of *y*-response at the disk

3.2.4 Impact of the seal length L_s

Fig. 13 describes the characteristics of system motion when the seal length is adopted as the bifurcation parameter and ranges from 30 to 80 mm, for r_d=0.06 mm, Δp=0.5 MPa and c_s=1 mm. The whole motion process can be summarized as: multiple periodic motion→quasi-periodic motion alternating with multiple periodic motion→quasi-periodic motion→periodic motion. The diagrams indicate that increasing seal length causes instability in the system. The multi-periodic motion becomes quasi-periodic motion at L_s=43 mm and the motion state transits between multiple periodic and quasi-periodic in the range [43, 62] mm. The amplitude of the system starts

to decrease at L_s=52 mm and the system becomes periodic motion when the seal length is larger than 62 mm.

3.2.5 Impact of the mass eccentricity of the disk r_d

Fig. 14 shows the characteristics of system motion when the mass eccentricity of the disk is adopted as the bifurcation parameter and ranges from 0.001 to 0.08 mm, for L_s=52 mm, Δp=0.5 MPa, and c_s=1 mm. The whole motion process is summarized as follows: periodic motion→quasi-periodic motion→quasi-periodic motion alternating with chaotic motion →double-periodic motion. The system remains stable at small mass eccentricities (r_d<0.055 mm). However, at r_d=0.055 mm, the system bifurcates into quasi-periodic motion and the amplitude increases rapidly. In the range [0.055, 0.073] mm, the system shifts between quasi-periodic and chaotic motion. When r_d=0.073 mm, double-periodic motion occurs.

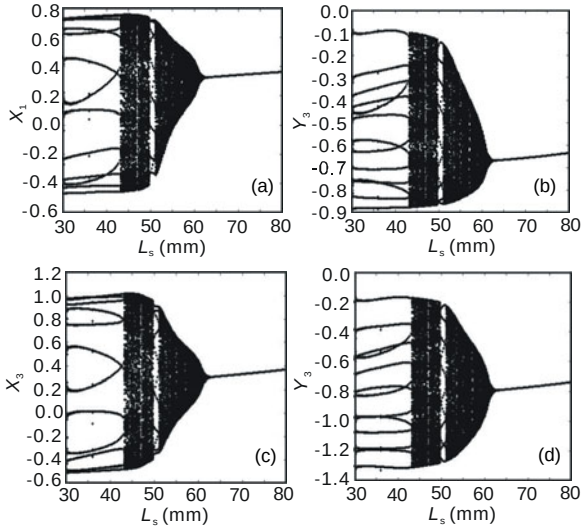

Fig. 13 Bifurcation behavior of the rotor with increasing seal length

(a) Bifurcation of *x*-response at the bearing; (b) Bifurcation of *y*-response at the bearing; (c) Bifurcation of *x*-response at the disk; (d) Bifurcation of *y*-response at the disk

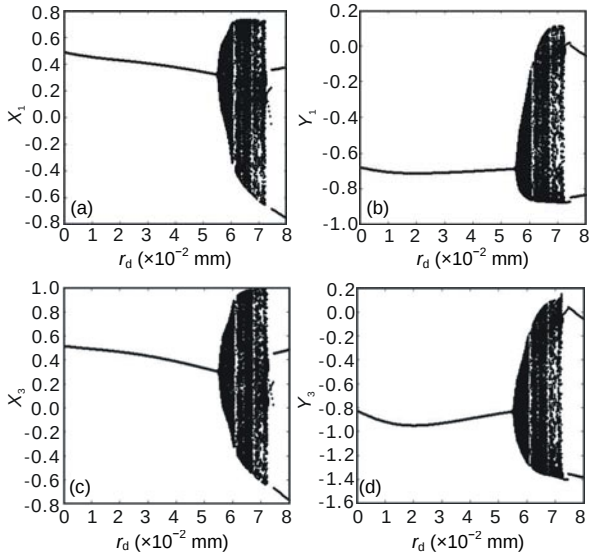

Fig. 14 Bifurcation behavior of the rotor with increasing mass eccentricity of the disk

(a) Bifurcation of *x*-response at the bearing; (b) Bifurcation of *y*-response at the bearing; (c) Bifurcation of *x*-response at the disk; (d) Bifurcation of *y*-response at the disk

4 Conclusions

We presented a numerical analysis of the nonlinear dynamic characteristics of a rotor/bearing/seal system with the coupled effects of the nonlinear oil film force and the nonlinear seal force. A new dynamic equation for the rotor system has been established based on the Hamilton principle and the FEM. The equations of motion have been solved effectively using the fourth order Runge-Kutta method. The dynamic response of the rotor system has been examined in detail using bifurcation diagrams, Lyapunov exponents, phase trajectory diagrams, and Poincaré maps. The numerical results show that the rotational speed of the rotor, the pressure drop in the seal, the seal length, the seal clearance, and the mass eccentricity of the disk are the key parameters, which significantly affect the dynamic characteristics of the rotor system. With the coupled effects of the nonlinear oil film force, the nonlinear seal force, and the mass eccentricity of the disk, the motion of the rotor system shows complicated nonlinearity. It exhibits complex types of periodic, quasi-periodic, double-periodic, multi-periodic, and chaotic vibrations. The discovery of these forms of vibrations could be helpful in further studies of nonlinear vibration in rotor/bearing/seal systems.

References

Al-Nahwi, A.A., Paduano, J.D., Nayfeh, S.A., 2003. Aerodynamic-rotordynamic interaction in axial compression systems-part II: impact of interaction on overall system stability. *Journal of Turbomachinery*, **125**(3): 416-424. [doi:10.1115/1.1576431]

Chang-Jian, C.W., 2010a. Non-linear dynamic analysis of dual

flexible rotors supported by long journal bearings. *Mechanism and Machine Theory*, **45**(6):844-866. [doi:10.1016/j.mechmachtheory.2009.11.010]

Chang-Jian, C.W., 2010b. Nonlinear analysis for gear pair system supported by long journal bearings under nonlinear suspension. *Mechanism and Machine Theory*, **45**(4):569-583. [doi:10.1016/j.mechmachtheory.2009.11.001]

Chang-Jian, C.W., Chen, C.K., 2006a. Bifurcation and chaos of a flexible rotor supported by turbulent journal bearings with non-linear suspension. *Proceedings of the Institution of Mechanical Engineers, Part J: Journal of Engineering Tribology*, **220**(6):549-561. [doi:10.1243/13506501JET167]

Chang-Jian, C.W., Chen, C.K., 2006b. Nonlinear dynamic analysis of a flexible rotor supported by micropolar fluid film journal bearings. *International Journal of Engineering Sciences*, **44**(15-16):1050-1070. [doi:10.1016/j.ijengsci.2006.06.008]

Chang-Jian, C.W., Chen, C.K., 2007a. Chaos and bifurcation of a flexible rub-impact rotor supported by oil film bearings with non-linear suspension. *Mechanism and Machine Theory*, **42**(3):312-333. [doi:10.1016/j.mechmachtheory.2006.03.007]

Chang-Jian, C.W., Chen, C.K., 2007b. Bifurcation and chaos analysis of a flexible rotor supported by turbulent long journal bearings. *Chaos Solitons and Fractals*, **34**(4):1160-1179. [doi:10.1016/j.chaos.2006.04.021]

Cheng, M., Meng, G., Jing, J.P., 2007a. The nonlinear dynamical behaviors of a rotor-bearing-seal system. *Journal of Shanghai Jiaotong University*, **41**(3):398-403 (in Chinese).

Cheng, M., Meng, G., Jing, J.P., 2007b. Numerical and experimental study of a rotor-bearing-seal system. *Mechanism and Machine Theory*, **42**(8):1043-1057. [doi:10.1016/j.mechmachtheory.2006.04.010]

Cheng, M., Meng, G., Jing, J.P., 2008. Numerical analysis of nonlinear rotor-bearing-seal system. *Journal of Shanghai Jiaotong University (Science)*, **13**(4):418-425. [doi:10.1007/s12204-008-0418-8]

Huang, L., Huang, P.W., Liu, Y.H., Wei, J.L., Qiu, Y.J., Jiang, B.H., 2007. Study of nonlinear dynamic characteristics of turbine rotor system under oil-film force, Alford force and quality eccentricity. *Turbine Technology*, **49**(6):428-431, 438 (in Chinese).

Li, Z.G., 2007. Research on the Nonlinear Dynamic Characteristics of a Rotor-Bearing-Seal System. MS Thesis, Harbin University of Technology, Harbin, China (in Chinese).

Luo, T.S., Wang, S.L., Guo, Y.M., 2007. Application of high-dimensional dynamic system in rotor stability analysis. *Journal of Zhejiang University (Engineering Science)*, **41**(6):959-962 (in Chinese).

Mei, F.X., Liu, J.L., 1987. Introduction to Analysis Mechanics. Xi'an Jiaotong University Press, Xi'an, China (in Chinese).

Muszynska, A., Bently, D.E., 1990. Frequency-swept rotating input perturbation techniques and identification of the fluid force models in rotor/bearing/seal systems and fluid handling machines. *Journal of Sound and Vibration*, **143**(1):103-124. [doi:10.1016/0022-460X(90)90571-G]

Rosenstein, M.T., Collins, J.J., de Luca, C.J., 1993. A practical method for calculating largest Lyapunov exponents from small data sets. *Physica D: Nonlinear Phenomena*, **65**(1-2):117-134. [doi:10.1016/0167-2789(93)90009-P]

Shen, X.Y., 2007. Study on Vibration of Ultra Supercritical Turbine Rotor Systems and Nonlinear Dynamics of Several Rotor Systems with Faults. PhD Thesis, Shanghai Jiao Tong University, Shanghai, China (in Chinese).

Wang, L.P., Li, X.F., Shi, T.L., Yang, S.Z., 1999. Nonlinear dynamic model of continuous rotor systems. *Turbine Technology*, **41**(2):97-99 (in Chinese).

Wang, W.Z., Liu, Y.Z., Meng, G., Jiang, P.N., 2009. Nonlinear analysis of orbital motion of a rotor subject to leakage air flow through an interlocking seal. *Journal of Fluids and Structures*, **25**(5):751-765. [doi:10.1016/j.jfluidstructs.2008.07.009]

Wang, Y.F., Wang, X.Y., 2010. Nonlinear vibration analysis for a Jeffcott rotor with seal and air-film bearing excitations. *Mathematical Problems in Engineering*, Article 657361, p.1-14. [doi:10.1155/2010/657361]

Xu, X.F., Zhang, W., 2000. Bifurcation and chaos of rigid unbalance rotor in short bearings under an unsteady oil film force model. *Journal of Vibration Engineering*, **13**(2):247-252 (in Chinese).

Zeng, P., 2004. Finite Element Analysis and Applications. Tsinghua University Press, Beijing (in Chinese).

Zhang, W., 1990. The Theoretical Base of Rotordynamic. Science Press, Beijing (in Chinese).